Astron. Astrophys. 342, 583–591 (1999)

ASTRONOMY AND ASTROPHYSICS

Yohkoh observations of the Neupert effect

M. Tomczak

Astronomical Institute, Wrocław University, Kopernika 11, PL-51-622 Wrocław, Poland (e-mail: tomczak@astro.uni.wroc.pl)

Received 18 February 1998 / Accepted 4 November 1998

Abstract. A Neupert effect is a well-known observational aspect of dynamics of many solar flares during their impulsive phase. Imaging capabilities of the *Yohkoh* satellite provide a new perspective in an investigation of this effect. In this paper it has been shown that impulsive soft X-ray brightenings are a direct cause of some soft X-ray excess resulting as the Neupert effect. An additional observational confirmation is presented that the impulsive phase of flares showing the Neupert effect is dominated by non-thermal electron beams. The importance of relatively soft (below 10 keV) non-thermal electrons in the production of soft X-ray brightenings is suggested.

Key words: Sun: X-rays, gamma rays – Sun: flares – Sun: corona

1. Introduction

Neupert (1968) reported that during the impulsive phase of some solar flares the value of the soft X-ray flux increment closely matches a total hard X-ray light curve. Such a relationship, called the Neupert effect, can be described by the following simple formula:

$$\partial F_{\rm SXR}/\partial t = kF_{\rm HXR} \quad (1)$$

where $F_{\rm SXR}$ and $F_{\rm HXR}$ are fluxes emitted by a flare during the impulsive phase in soft and hard X-rays respectively. The value of the coefficient k changes with the evolution of a flare and is not identical for different events. For these purposes we should treat the Neupert effect as a qualitative relationship between soft and hard X-ray emission of flares rather than a strict formula.

A satisfactory physical explanation of the Neupert effect is provided by a thick-target model (Brown 1971). As one of the results of energy release in a coronal part of a flaring magnetic structure non-thermal electrons are accelerated in the impulsive phase. These particles propagate along magnetic field lines and precipitate into the footpoints, i.e. the denser part of the solar atmosphere, where the flaring structure is rooted. Non-thermal electron beams are stopped there emitting hard X-ray radiation via bremsstrahlung and heating the environment by the Coulomb collisions. Energetically, only a small fraction ($\simeq 3 \times 10^{-6}$) of the non-thermal electron energy is emitted as bremsstrahlung radiation (Tandberg-Hanssen & Emslie 1988).

The energy deposited by non-thermal electrons quite easily heats the plasma in the footpoints to a temperature of several millions K. Thermal emission of this plasma gives some additional contribution to the soft X-ray radiation of the flare. Such a contribution we observe as the Neupert effect.

Previous investigations of the Neupert effect have provided some confirmation of the above physical explanation (Dennis & Zarro 1993, and references therein). For example, it has been shown that only for type B flares in the hard X-ray classification of flares proposed by Tanaka (1983) the Neupert effect is observed. It has been generally agreed that the impulsive phase of these flares is described very well by the thick-target model. On the other hand, for type A and C flares, other mechanisms of the hard X-ray emission are proposed and these flares do not show the Neupert effect.

Although this physical interpretation of the Neupert effect has good observational and theoretical support, former instruments do not offer a direct proof for it. The Japanese satellite *Yohkoh* (Ogawara et al. 1991) has been providing sufficient technical parameters to investigate the Neupert effect in a new perspective. In Sect. 2 I present the observational evidence that supports the above physical interpretation of the Neupert effect. In Sect. 3 I use the imaging capabilities of *Yohkoh* to verify the thick-target model.

2. The Neupert effect seen on the *Yohkoh* images

Yohkoh has two imaging instruments observing the Sun in X-rays. The Soft X-ray Telescope (Tsuneta et al. 1991), SXT, is a grazing-incidence telescope sensitive to 0.4–4.2 keV soft X-rays, having a CCD detector and filters to provide wavelength discrimination. During a flare mode the SXT usually performs frames that consist of 64 $\times$ 64 2.45 arcsec pixels taken sequentially every 2 s by the following filters: a 119 μm beryllium filter (Be119), a 11.6 μm Al filter (Al12) and a 1265 Å Al filter (Al.1). In various observational schemes a repetition of the same filter is every 4–12 s.

The Hard X-ray Telescope (Kosugi et al. 1991), HXT, is a Fourier-synthesis hard X-ray imager which measures spatially modulated intensities from 64 independent subcollimators in four energy bands (L: 14–23 keV, M1: 23–33 keV, M2: 33–53 keV, and H: 53–93 keV). During a flare mode these intensi-

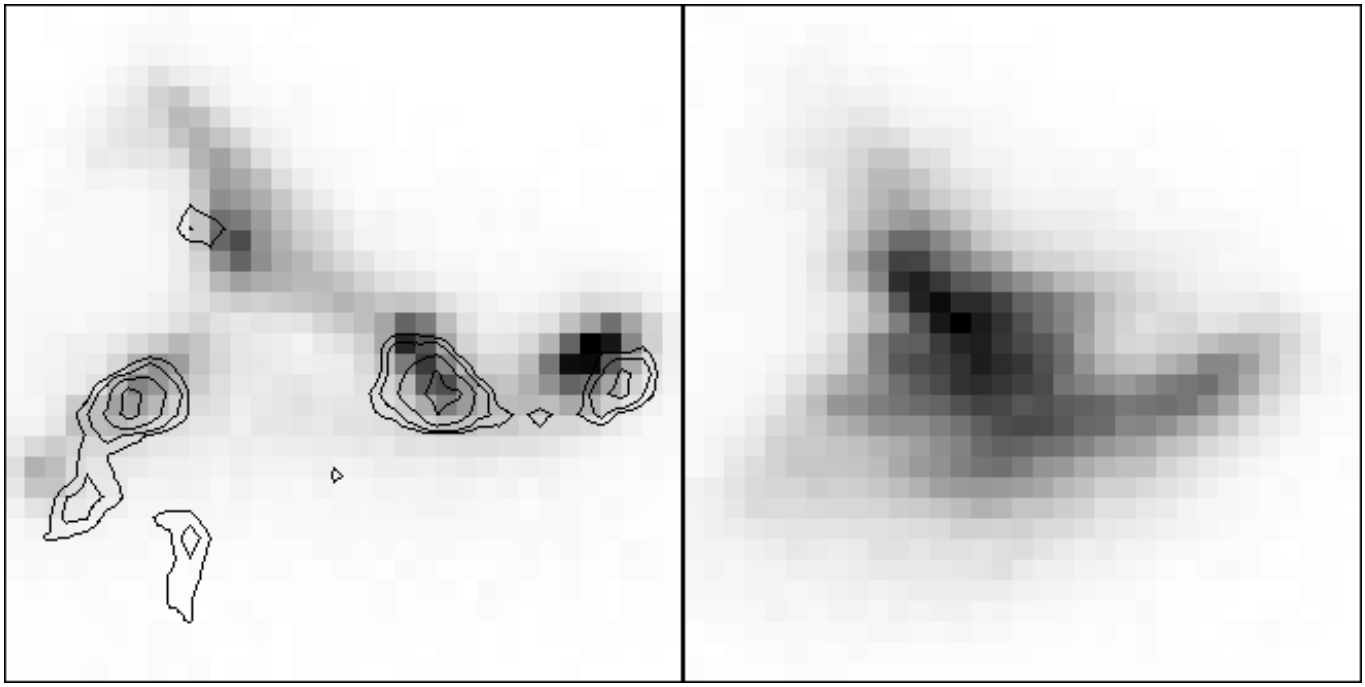

Fig. 1. Two images of the 14 February 1992 flare. The field of view is 81 arcsec × 81 arcsec. Solar north is up, east to the left. The SXT(Be119) emission distribution is represented by a grey scale determined by the brightest pixel. The size of each pixel is 2.45 arcsec. Contours of the HXT(M2) emission (78.4, 39.2, 19.6 and 11.8% of the maximum intensity) are overplotted. The left image was taken at 23:07:30 UT – the maximum of the main hard X-ray burst. The right image was made at 23:10:30 UT – the maximum of the SXT(Be119) flux.

ties are measured every 0.5 s. Some routines are available (e.g. MEM, pixon) that allow the reconstruction of the hard X-ray distribution with an angular resolution of up to 5 arcsec. The time resolution depends on the number of counts.

During the impulsive phase of many flares the SXT images show impulsive soft X-ray brightenings (Strong et al. 1993; Hudson et al. 1994b; Tomczak 1997a, 1997b). There are sudden jumps of emission observed at the footpoints of the flaring structures. The good temporal and spatial correlations between impulsive soft X-ray brightenings and hard X-ray footpoint emission sources indicate a common physical source – non-thermal electron beams. The hard X-ray radiation is the bremsstrahlung of non-thermal electrons when they impact against the denser environment. The thermal nature of the impulsive soft X-ray brightenings indicates that this is radiation of the environment heated by non-thermal electron beams (Hudson et al. 1994b).

In this section I show that the impulsive soft X-ray brightenings are directly responsible for the additional emission which temporary changes the value of the total soft X-ray flux increment. In other words, the impulsive soft X-ray brightenings produce the Neupert effect. I illustrate this statement by the *Yohkoh* images of two flares. The first one, of 14 February 1992, has extra strong soft X-ray brightenings, the second one, of 13 January 1992, has relatively simple morphology.

2.1. The 14 February 1992 flare

The M7.0/2B flare occurred on 14 February 1992, in NOAA Active Region 7056, close to the central meridian (S13 E02). Its

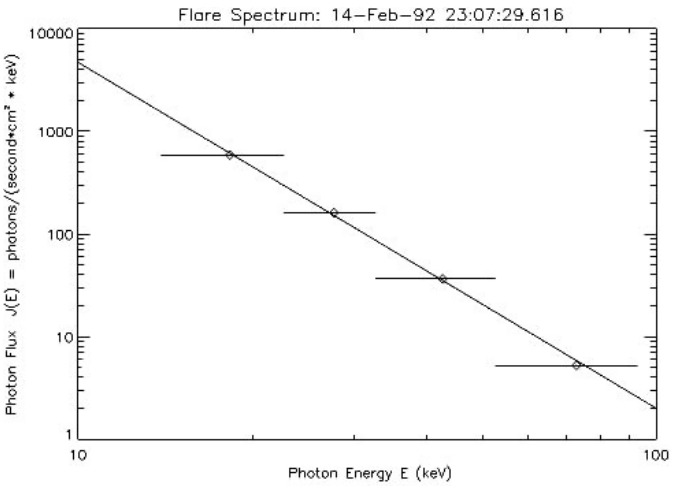

Fig. 2. The total photon flux spectrum of the 14 February 1992 at the maximum of hard X-rays. Plane bars represent energy bands of the HXT channels. A single power-law fit is drawn.

GOES maximum was about 23:10 UT. A preliminary analysis of this event was presented by Hudson et al. (1994a). Fig. 1 presents two images of the flare taken at the maximum of hard X-rays (left) and at the maximum of soft X-rays (right). In both images the spatial distribution of the soft X-ray emission is shown by a grey scale. A detailed analysis of the whole available sequence of the soft X-ray images suggests that this flare was located in a complicated magnetic structure resembling a circus tent. During the impulsive phase (Fig. 1, left image) strong soft

Table 1. Parameters of the investigated flares during the main hard X-ray burst

Parameter	13-JAN-92	14-FEB-92
From the HXT data		
Power-law index, γ	4.1	3.4
Parameter A_1 in Eq. 2	3.6×10^6	1.1×10^7
Total energy flux of non-thermal electrons, $\mathcal{F}(E \geq 14$ keV) [ergs s^{-1}]	6.3×10^{28}	8.9×10^{29}
Duration of impulsive onset, Δt [s]	40	15
Total energy deposition by the $E \geq 14$ keV electrons, (1/2)$\mathcal{F}(E \geq 14$ keV$) \times \Delta t$ [ergs]	1.2×10^{30}	6.6×10^{30}
From the SXT data (mean values for the footpoints showing impulsive soft X-ray brightenings)		
Temperature, T [MK]	8.6	8.8
Emission measure, ε [cm^{-3}]	2.0×10^{48}	1.7×10^{49}
Total raditive energy loss, $\varepsilon\Phi(T)$ [ergs s^{-1}]	8×10^{25}	8×10^{26}
Estimated mean density of the plasma, $\bar{N}$ [cm^{-3}]	7×10^{10}	1.2×10^{11}
Contained thermal energy, $3\varepsilon kT/\bar{N}$ [ergs]	1.0×10^{29}	5.2×10^{29}

X-ray brightenings at the footpoints of this tent-like structure distinctly dominated the emission of the whole structure. Three minutes later (Fig. 1, right image), the evaporated plasma filled the whole flaring structure and a bright emission kernel at the top of the structure was formed.

Fig. 2 shows the total photon flux spectrum recorded by the HXT at the maximum of hard X-rays. We see that the counts of all four channels can be described by a single power-law formula with a satisfying accuracy. This result strongly suggests that the whole HXR emission ($h\nu \geq 14$ keV) was produced by non-thermal electron beams.

On the left image of Fig. 1 contours of the hard X-ray emission observe in the HXT channel M2 are overplotted. I found that the prominent hard X-ray emission sources are located at the footpoints of the flaring magnetic structure. Such a location suggests an interpretation of the hard X-ray radiation as thick-target emission of non-thermal electrons.

In Table 1 are presented parameters of the single power-law fit from Fig. 2. I used the following formula:

$$I(E) = A_1 E^{-\gamma} \qquad \text{photons} \times \text{cm}^{-2}\text{s}^{-1}\text{keV}^{-1} \tag{2}$$

where I is the photon flux at an energy E in keV, γ is a power-law index and A_1 is a constant. According to the thick-target model the total energy flux of non-thermal electrons above the cut-off energy E_0 is given by the following formula (Crosby et al. 1993):

$$\mathcal{F}(\geq E_0) \; = \; 4.8 \times 10^{24} A_1 E_0^{-\gamma+1} \gamma(\gamma-1) B(\gamma - 0.5, 0.5) \quad \text{ergs} \times \text{s}^{-1} \tag{3}$$

where B is the beta function. In the considered case the calculated total energy flux of non-thermal electrons having energies above 14 keV was 8.9×10^{29} ergs s^{-1}.

During the main hard X-ray burst of the 14 February 1992 flare the footpoints with strong hard X-ray emission showed also distinct impulsive soft X-ray brightenings. A very good temporal and spatial correlation between the sources of hard X-ray emission and areas of impulsive soft X-ray brightenings strongly suggests a common origin – non-thermal electron beams. From the SXT images I estimated a total radiative energy loss of the footpoints showing impulsive soft X-ray brightenings (see Table 1). The derived value is about three orders lower than the total energy flux of non-thermal electrons. I compared also the thermal energy contained in the footpoints showing impulsive soft X-ray brightenings and the total energy deposition in non-thermal electrons having energies above 14 keV. As we can see, in Table 1, the first quantity is distinctly lower than the second. The above comparisons confirm that non-thermal electrons have deposit enough energy at the footpoints to produce the HXR emission and the impulsive soft X-ray brightenings.

A detailed investigation of SXT light curves seems to be a very efficient way for localizing places of non-thermal-electron precipitation (Tomczak 1997a, 1997b). As the consequence of heating by non-thermal electrons such places in SXT images show the impulsive maximum of a light curve. I selected SXT pixels showing a clear response to the non-thermal electron beams during the period of the main hard X-ray burst. For this purpose, I carefully inspected light curves of individual pixels choosing those which reach their maximum intensity at the time of the main hard X-ray maximum or several seconds later. I inspected the light curves for each SXT filter under consideration. All together, I selected 70 pixels which fulfilled the above criterion. These pixels occupied about 10% of the whole SXT flaring area and during the main hard X-ray burst they produced up to 30% of the whole SXT emission.

The aggregated SXT(Be119) light curve for all 70 selected pixels is plotted as triangles in the upper panel of Fig. 3. In the same panel are shown also two other light curves of the whole flaring structure (crosses) and of the whole flaring structure except for those 70 selected pixels (diamonds) respectively. The

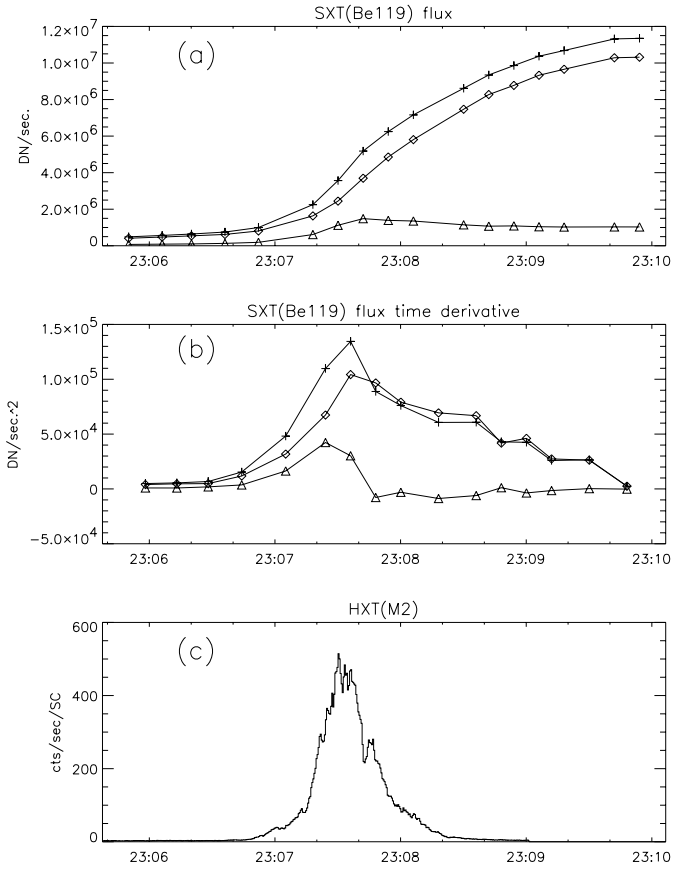

Fig. 3a–c. Some plots for the 14 February 1992 flare. **a** The SXT(Be119) light curves summed up over all 70 selected brightened pixels (triangles), for the whole flaring structure (crosses) and for the whole flaring structure without selected pixels (diamonds). **b** The SXT(Be119) light curve time derivatives for the selected pixels (triangles), for the whole flaring structure (crosses) and for the whole flaring structure without selected pixels (diamonds). **c** The HXT(M2) light curve.

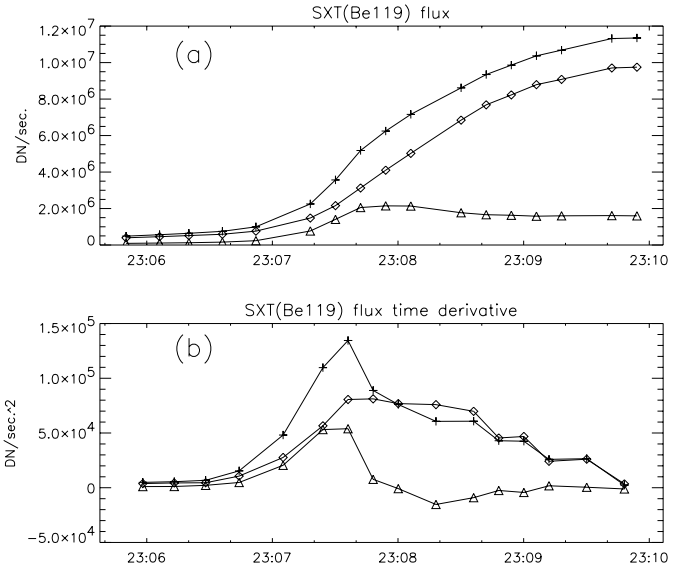

Fig. 4a and b. The same as Fig. 3a–b but after including additional 31 SXT pixel reaching a maximum of brightness during the impulsive phase outside the period of the main hard X-ray burst.

curve for the selected brightened pixels has a completely different appearance from the two others in the upper panel. On the other hand, a similarity between this curve and the HXT(M2) curve (Fig. 3, lower panel) is evident.

In the middle panel of Fig. 3 the SXT(Be119) light curve time derivatives are shown. As in the upper panel, triangles show the curve for 70 selected brightened pixels in the footpoints, crosses show the curve for the whole flaring structure and diamonds – for the whole flaring structure except these selected pixels. The curves for the triangles and crosses resemble the HXT(M2) light curve very well. After subtracting the signal of 70 selected pixels from the total signal, the SXT(Be119) light curve time derivative shows a much worse resemblance to the HXT(M2) light curve. This means that I have found the part of the flaring structure responsible for the Neupert effect. It consists of the footpoints showing impulsive soft X-ray brightenings.

Despite the above conclusion, the correspondence between the SXT(Be119) light curve time derivative for the whole flaring structure except 70 selected pixels and the HXT(M2) light curve is still visible. This means that other parts of the flaring structure also give some contribution to the Neupert effect. Two explanations are possible. First, during the whole impulsive phase other areas of impulsive soft X-ray brightenings existed which were not detected within the period of the main hard X-ray burst (Tomczak 1997a, 1997b). Indeed, after including the SXT pixels reaching their maximum brightness in the impulsive phase outside the period of the main hard X-ray burst, the correspondence between the SXT(Be119) light curve time derivative for the whole flaring structure except selected pixels and the HXT(M2) light curve is definitely worse (see Fig. 4).

The second explanation is that the used method for searching the area of response was too strict because it could not incorporate the pixels in which some non-thermal electron heating exists, but did not produce a detectable maximum in the SXT images. At first sight, a key is to investigate the light curve time derivative for the individual pixels. However, usually a limitation for that is poor statistics. As a consequence, some underestimation of the response of the footpoints on the non-thermal electron beams is possible.

2.2. The 13 January 1992 flare

The famous Masuda flare (Masuda 1994; Masuda et al. 1994, 1995) was observed on 13 January 1992. Its GOES maximum occurred at 17:34 UT. The flare was located in a simple magnetic loop on the solar west limb and had M2.0 class. Fig. 5 presents two SXT(Al12) images of this flare, one at the period of the main hard X-ray burst and another at the maximum of the SXT(Al12) light curve (7 minutes later). In the left frame contours of the HXT(M2) emission are plotted.

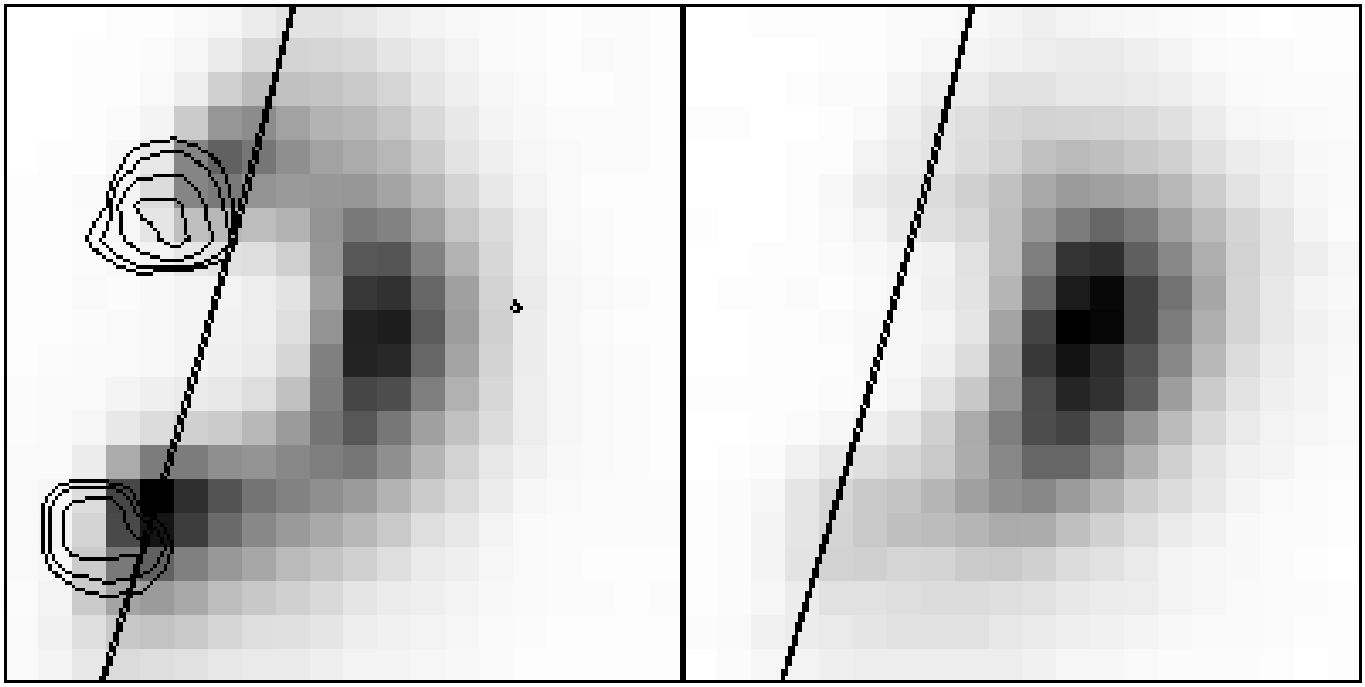

Fig. 5. Two SXT(Al12) images of the 13 January 1992 flare are presented. The field of view is 49 arcsec × 49 arcsec. The left image was taken within the period of the main hard X-ray burst, at 17:28:13 UT. Contours of the HXT(M2) emission are overplotted. The right image was made at 17:35:15 UT – the maximum of the SXT(Al12) flux. The continuous line represents the solar west limb. For other details – see the caption of Fig. 1.

As in the case of the 14 February 1992 flare the total hard X-ray photon flux spectrum during tha main hard X-ray burst can be descibed by a single power-law formula (Fig. 6). Moreover, we see that the hard X-ray emission is concentrated in the footpoints of the flaring loop (Fig. 5). An impulsive loop-top hard X-ray emission source reported in Masuda's papers was dominated at that time by the footpoint sources and therefore it was difficult to detect (Masuda 1994 – note that the impulsive loop-top source was clearly seen earlier than the peak time when the relative contribution of this source to the whole hard X-ray emission was more important.) Impulsive soft X-ray brightenings observed during the main hard X-ray burst were also located in the footpoints. In summary, the shape of the photon flux spectrum, the location of the hard X-ray emission and very good temporal and spatial correlation between impulsive soft X-ray brightenings and hard X-ray emission sources show again that at the time of the main hard X-ray burst in the footpoints of the flaring loop non-thermal electron beams were stopped. Also a comparison between calculated parameters presented in Table 1 confirms that non-thermal electrons deposited enough energy at the footpoints to produce the HXR emission and the impulsive soft X-ray brightenings.

In the same way as for the 14 February 1992 flare I showed that impulsive soft X-ray brightenings are directly responsible for the Neupert effect. For the evidence – see Fig. 7. In the upper panel of this figure are presented three aggregated SXT(Al12) light curves for all pixels reaching a maximum brightness during the main hard X-ray burst (triangles, 24 selected pixels), for the whole flaring structure (crosses) and for the whole flaring

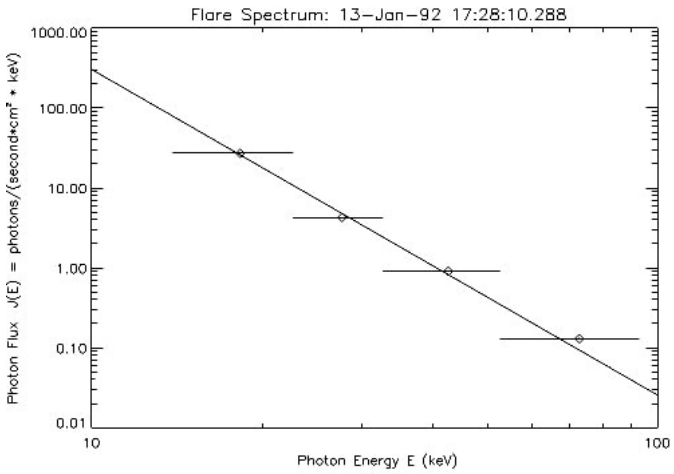

Fig. 6. The total photon flux spectrum of the 13 January 1992 at the maximum of hard X-rays. For other details – see the caption of Fig. 2.

structure excluding these 24 pixels (diamonds), respectively. The SXT(Al12) flux time derivative (middle panel) for the whole flaring structure shows definitely a closer similarity to the HXT(M2) light curve (bottom panel) than the SXT(Al12) flux time derivative for the whole flaring structure except the selected pixels. Further jumps in the SXT(Al12) flux time derivative (after 17:29 UT) are probably not real and have some instrumental reasons (e.g. some uncertainties of image coalignment caused by jitter in the satellite pointing – see Siarkowski et al. 1996).

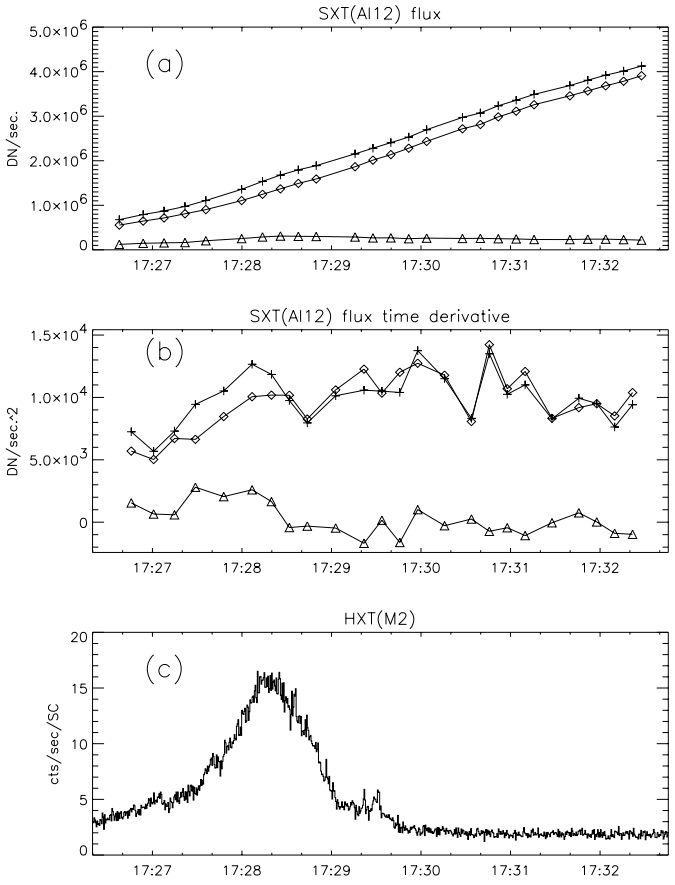

Fig. 7a–c. Some plots for the 13 January 1992 flare. **a** The summary SXT(Al12) light curves for all 24 selected brightened pixels (triangles), for the whole flaring structure (crosses) and for the whole flaring structure without selected pixels (diamonds). **b** The SXT(Al12) light curve time derivatives for all 24 selected brightened pixels (triangles), for the whole flaring structure (crosses) and for the whole flaring structure without selected pixels (diamonds). **c** The HXT(M2) light curve.

3. Observational test of the thick-target model

Thanks to the *Yohkoh* telescopes, SXT and HXT, we have a unique opportunity to observe simultanously two consequences of non-thermal electron precipitation during the impulsive phase of the solar flares. These are the hard X-ray bremsstrahlung and the soft X-ray response of the heated footpoints. A comparison of them can provide a new observational test of the thick-target model.

I selected five flares that were well-observed by *Yohkoh*. Basic parameters of these flares are presented in Table 2. Each event from the list has a typical impulsive phase which consists of several hard X-ray bursts (e.g. Figs. 3c and 7c). At these times soft X-ray brightenings can be seen in the SXT images.

I considered the period of the main hard X-ray burst only, when the strongest influence of the non-thermal electron beams was expected. In Sect. 2 I showed that such beams are responsible for the HXR emission and impulsive soft X-ray brightenings in the case of events 2 and 4 from Table 2. This is the case also for the other events from Table 2. The evidence is the same

Table 2. List of selected flares

Event Number	Date	GOES max. time [UT]	Importance	Coordinates
1	Nov 19, 91	09:32	C8.5/1F	S12 W60
2	Jan 13, 92	17:34	M2.0/–	S15 Wlimb[a]
3	Jan 26, 92	15:33	X1.0/3B	S16 W66
4	Feb 14, 92	23:10	M7.0/2B	S13 E02
5	Feb 17, 92	15:46	M1.9/SF	N16 W81

[a] Coordinates estimated from SXT images

as that presented in Sect. 2: the single power-law shape of the total HXT photon flux spectrum, the location of strong hard X-ray sources at the footpoints of the flaring structure and very good temporal and spatial correlation between these hard X-ray sources and impulsive soft X-ray brightenings.

In Table 3 I summarized the obtained response to the non-thermal electron beams in the footpoints of the events listed in Table 2. Values are given for the individual identified footpoints and mean values for the complete events. I selected a time interval near the main hard X-ray burst maximum long enough to synthesize a hard X-ray image taken by one of the more energetic HXT channels. For a quantitative analysis I selected channel M1 and M2 images only. Such a choice seems to be the safest because the HXT(H) images have sometimes a very noisy nature and the HXT(L) images show sometimes, even in the impulsive phase, a significant contribution from regions other than the footpoints.

Photometry using HXT images is disturbed by some spurious sources produced by any used reconstruction technique (Metcalf et al. 1996, Alexander & Metcalf 1997). Fortunately, during the main burst the hard X-ray emission of flares is dominated by footpoint sources (e.g. Sakao 1994, see also the samples in Sect. 2). In my analysis, any faint hard X-ray sources (consisting of pixels having an intensity below 10% of the most intense pixel) I treated as artificial and its signal was manually redistributed between the strong sources. For the HXT images reconstruction I used an adaptation of the Maximum Entropy Method written by Sakao (1994). A repeated calculation with new HXT instrument response functions (Sato 1997) derived similar results. The number of HXT counts from the individual footpoints and for the whole events are presented in Table 3.

As an area of the soft X-ray response at the footpoints were selected the pixels reaching their maximum of brightness within the period of the main hard X-ray burst or several seconds later. Such an investigation was made for the SXT images obtained with Be119, Al12 and Al.1 filters. Impulsive soft X-ray brightenings were most evident in the Al12 filter. Therefore, I chose this filter for a quantitative analysis of the soft X-ray response.

A difficult task was to distinguish between the influences of non-thermal electron beams and other origins (both physical e.g. thermal conduction and instrumental) of the soft X-ray emission in the footpoints. For this purpose, I estimated the range of the SXT(Al12) response due to non-thermal electron

Table 3. Response to the non-thermal electron beams in the footpoints of flares from Table 2

Event Number[a]	Date	HXT Integration Time [UT]	HXT(M1) [cts cm^{-2} s^{-1}]	HXT(M2)	Estimated range of SXT(Al12) response [DN s^{-1}]	power-law index (γ)
1	Nov 19, 91	09:28:30.5-09:28:43.5	9.7	4.0	2.2–3.4 $\times 10^5$	4.3
1.1		the same	3.8	1.0	0.8–1.6 $\times 10^5$	5.6
1.2		the same	5.8	3.0	1.0–1.8 $\times 10^5$	3.6
2	Jan 13, 92	17:28:10.3–17:28:30.3	26.5	14.9	1.3–3.2 $\times 10^5$	3.4
2.1		the same	14.7	9.1	4.8–9.4 $\times 10^4$	3.2
2.2		the same	11.8	5.8	0.8–2.3 $\times 10^5$	3.8
3	Jan 26, 92	15:28:34.1–15:28:35.1	692.3	388.8	1.9–3.7 $\times 10^6$	3.4
3.1		the same	242.2	163.0	0.4–1.4 $\times 10^6$	2.9
3.2		the same	331.9	166.4	1.0–1.7 $\times 10^6$	3.7
4	Feb 14, 92	23:07:29.6–23:07:30.6	957.6	576.0	1.9–2.8 $\times 10^6$	3.2
4.1		the same	394.6	227.4	4.9–6.7 $\times 10^5$	3.4
4.2		the same	338.8	232.8	3.1–5.9 $\times 10^5$	2.9
4.3		the same	194.4	93.3	1.0–1.3 $\times 10^6$	3.9
5	Feb 17, 92	15:40:45.1–15:41:00.1	11.9	5.7	1.1–3.0 $\times 10^5$	3.9
5.1		the same	7.7	4.0	1.0–1.9 $\times 10^5$	3.6
5.2		the same	4.2	1.7	0.4–1.1 $\times 10^5$	4.3

[a] The lines with single digits contain total values for the complete events, the others – for the individual footpoints of the same event. Sometimes the sum of the component values does not give the total value. It means that other footpoints were detected, too weak for separate analysis.

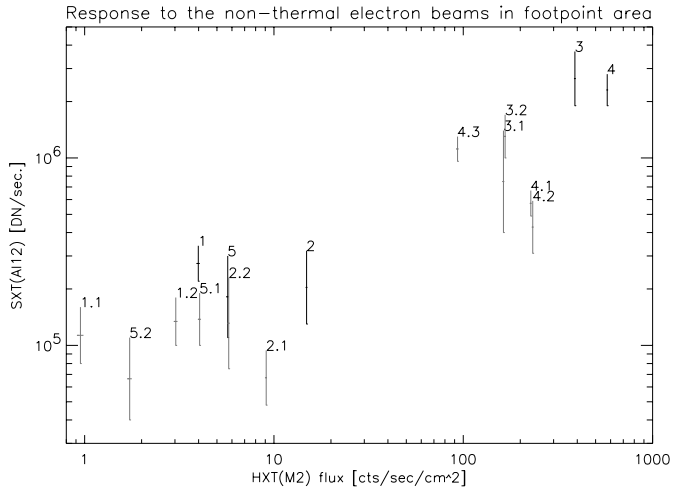

Fig. 8. Relation between two kinds of response to the non-thermal electron beams in footpoints observed in HXT(M2) channel and SXT(Al12) filter. The values and descriptions are taken from Table 3. See text for further details.

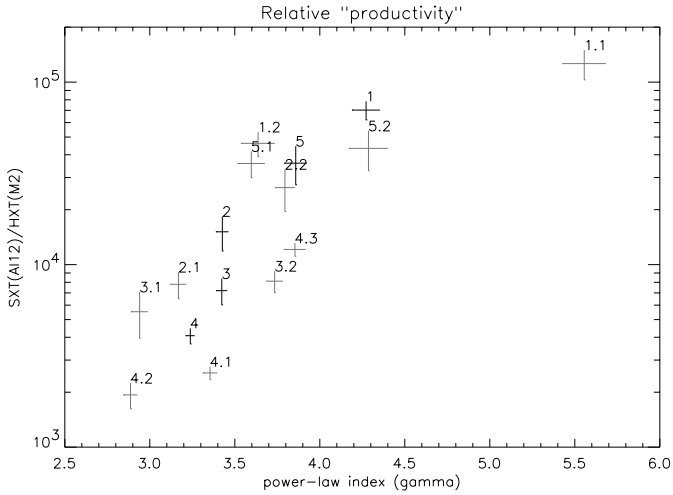

Fig. 9. Plot of relative productivity of soft X-rays SXT(Al12) with regard to hard X-rays HXT(M2) and power-law indexes that were estimated from the hardness ratio M2/M1. All values are taken from Table 3. The uncertainties are purely statistical.

beams. These ranges are given in Table 3. The upper limit is the value of the emission at the maximum of the aggregated light curve for all selected pixels. In other words, in the case of the upper limit I assumed that only non-thermal electron beams were responsible for the observed soft X-ray emission. The lower limit was calculated under the assumption that a contribution of these other origins than non-thermal electron beams of the soft X-ray emission of the footpoints was completely outside the impulsive phase, and rose linearly in time during the impulsive phase. As a result, the lower limit was the upper limit minus a background caused by these other origins, as estimated in the way described.

Fig. 8 presents a plot which summarises the responses to the non-thermal electron beams in the footpoints for the investigated flares. Hard X-ray intensities from channel M2 are plotted against the ranges of the soft X-ray response in the filter Al12, both taken from Table 3. The statistical errors of the hard X-ray intensities were also plotted. I would like to stress that the estimated ranges of the soft X-ray response can be considered as an maximal (3σ) error of the actual response. For easy identifi-

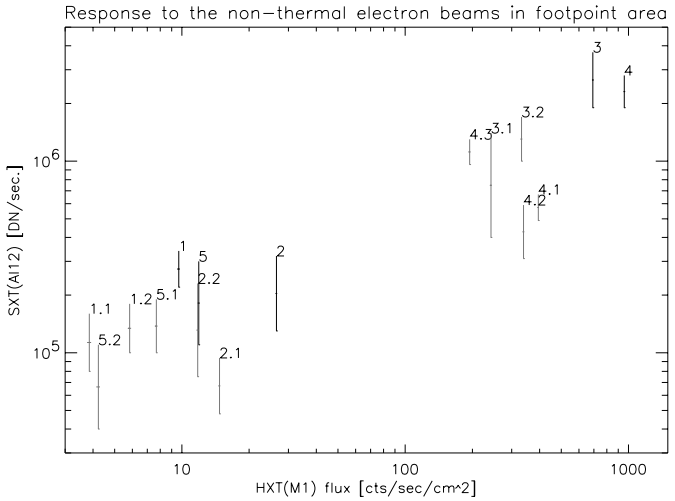

Fig. 10. Relation between two kinds of response to the non-thermal electron beams in footpoint observed in HXT(M1) channel and SXT(Al12) filter. The values and descriptions are taken from Table 3. See text for further details.

cation each point on the plot has the description number taken from Table 3.

There is a clear correlation seen in Fig. 8 which supports that both observables have a common physical reason, namely non-thermal electron beams. It means that this diagram gives an important observational evidence supporting the thick-target model. An observed scatter in the diagram can be explained as the result of observational uncertainties and errors in the method of analysis used.

However, there is some evidence suggesting that the observed scatter has a physical importance. The points representing individual footpoints of the same event are often situated along a line that is almost perpendicular to the general trend (e.g. 2.1 and 2.2 of the 13 January 92 flare, 4.1, 4.2 and 4.3 of the 14 February 92 flare). This anti-correlation is to some extend visible in Figs. 1a and 5a where the footpoints seen brighter in soft X-rays show lower hard X-ray emission.

I have found that the key for understanding this problem is a photon flux spectrum of hard X-rays. From the hardness ratio M2/M1 I calculated parameters of a single power-law formula fit. Obtained values of the power-law index are given in the last column of Table 3. By comparing values of the power-law index of events showing comparable soft X-ray responses and different hard X-ray intensities we see a clear dependence: lower γ (harder energy spectrum) is associated with higher hard X-ray intensity.

Supposing that the above dependence really exists, a quantity which measures the relative productivity of soft X-rays with regard to hard X-rays should depend on the power-law index. I divided the average value of the estimated range of the SXT(Al12) response by the HXT(M2) intensity for each event from Fig. 8. The results are plotted against the power-law index in Fig. 9. Statistical uncertainties of both plotted quantities were included. Each point is described by the number from Table 3. A clear correlation between these two quantities is seen. This means that the relative productivity of soft X-ray photons with regard to hard X-ray photons rises for higher γ (softer energy spectrum).

According to the thick-target model the energy spectrum of non-thermal electrons producing a power-law photon flux spectrum of hard X-rays via the bremsstrahlung has also a power-law shape with the index $\delta = \gamma + 1$. In other words, if we compare two energy spectra of hard X-rays having different indexes, the softer one is produced by non-thermal electrons with a softer energy spectrum.

Let us consider two non-thermal electron beams with different energy spectra producing the comparable values of the soft X-ray response. They produce also hard X-rays via the bremsstrahlung. Let us establish an energy range. If in this range a clear difference in hard X-ray intensities for both considered beams is observed (see samples on Fig. 8) it means that energetically different electrons produced the soft X-ray response and hard X-ray emission. Going toward lower energies the observed difference should be reduced because the energy spectrum of hard X-rays with higher value of index is steeper. As a matter of fact, a version of Fig. 8 with hard X-ray intensities taken from the lower energy channel M1 (Fig. 10) seems to have less scatter.

I extrapolated photon flux spectra of hard X-rays obtained for the investigated events (Table 3) toward lower energies and found that below 10 keV the correlation between photon flux and soft X-ray response is the best. (The scatter was lowest for the energy 8.7 keV). It suggests a common physical reason i.e. the non-thermal electrons producing the photons from this energy range are also responsible for the soft X-ray response. Keeping the above discussions in mind, we can conclude that the soft X-ray response of the footpoints heated by non-thermal electron beams and observed as impulsive soft X-ray brightenings is basically caused by relatively low energy electrons (below 10 keV).

Farnik et al. (1997) analyzed a series of flares of 3 October 1993 with exceptionally hard spectral indices in hard X-rays. For a first flare of the series at the top of the hard X-ray burst (09:06:50 UT) the authors reported a relative weakness of the soft X-ray response. This is in a good agreement with my results – the events that were relatively strong in hard X-rays with a flat spectrum (low value of γ) showed a relatively weak soft X-ray response. Farnik et al. also reported that the non-thermal bremsstrahlung spectra in the analyzed events may extend to a few keV. As evidence for this they showed the energy spectrum of photons taken at 09:06:50 UT where the low-energy extrapolation of the HXT intensities intersects counting rates from the Fe XXV (6.7 keV) and Fe XXVI (7.0 keV) channels of the *Yohkoh* Bragg Crystal Spectrometer. They examined the spectra to support that the BCS counts come from the continuum regions, not the emission lines. I believe that such a sample confirms that during the impulsive phase of some flares the non-thermal energy spectra of photons really extend to a few keV as I postulated in the above disscussion.

Another confirmation of my results comes from theoretical studies. Antonucci et al. (1993) simulated the response of a plasma confined in a coronal loop and heated by non-thermal electron beams. They used the numerical Palermo-Harvard code developed by Peres et al. (1982). They modified the parameters describing non-thermal electron beams and compared the response of the plasma. One of the conclusions from their paper was that the softer non-thermal electron beams (higher power-law index) produce the more evident soft X-ray plasma response (higher densities, emission measures, temperatures and velocities of evaporation) than the harder beams. Again, my results suggest the same dependence.

4. Conclusions

The *Yohkoh* instruments offer new possibilities to investigate physical phenomena occurring during the impulsive phase of the solar flares. I concentrated my attention on some observational manifestations of non-thermal electron beam precipitation in the footpoints of the flaring structures. The bremsstrahlung of the non-thermal electrons can be observed on the HXT images. The same electrons heat an environmental plasma to temperatures of a few million K. The thermal radiation of the heated plasma can be observed on the SXT images as impulsive soft X-ray brightenings.

I compared soft and hard X-ray emission caused by non-thermal electron beams for five well-observed flares. I found a proportionality between these parameters which supports their common physical origin. The scatter in Fig. 8 suggested a more complicated relationship. I found that the relative productivity of soft X-rays with regard to hard X-rays depends on the energy spectrum of hard X-ray photons, i.e. a steeper energy spectrum (higher power-law index) causes a higher soft X-ray productivity (Fig. 9). A main conclusion of the following discussion was that the soft X-ray response is produced basically by relatively low energy (below 10 keV) non-thermal electrons. This conclusion is also supported by other observational (Farnik et al. 1997) and theoretical (Antonucci et al. 1993) evidence.

I showed that impulsive soft X-ray brightenings are directly responsible for the Neupert effect. There is no doubt that when the soft X-ray images of flares with the SXT quality are available, a direct investigation of impulsive soft X-ray brightenings provides more details about the heating by non-thermal electron beams than the Neupert effect does. However, in the case of a lack of a SXT quality instrument, the Neupert effect provides a very important tool in the investigation of the impulsive phase of flares. But in such a case, keeping in mind the dependence of the Neupert effect on the power-law index of hard X-rays is advisable.

How do more energetic non-thermal electrons lose energy if they are not important in the soft X-ray response? Farnik et al. (1997) suggested that they reach the denser atmospheric layers, where most of their energy is lost through emission of UV radiation before it can drive strong outward flows.

Further theoretical and observational examination of the nature of the non-thermal electrons, including mechanisms like polarization, are postulated.

Acknowledgements. I acknowledge once more the great work of the whole *Yohkoh* Team. Their labour made this research possible. I thank Professors J. Jakimiec and K. J. H. Phillips for many useful comments and discussions. This work was supported by the British Council/KBN grant No. WAR/992/057 and by the KBN grant No. 2 P03D 016 14.

References

Alexander D., Metcalf T.R., 1997, ApJ 489, 442
Antonucci E., Dodero M.A., Martin R., et al. 1993, ApJ 413, 786
Brown J.C., 1971, Sol. Phys. 18, 489
Crosby N.B., Aschwanden M.J., Dennis B.R., 1993, Sol. Phys. 143, 275
Dennis B.R., Zarro D.M., 1993, Sol. Phys. 146, 177
Farnik F., Hudson H., Watanabe T., 1997, A&A 320, 620
Hudson H.S., van Driel-Gesztelyi L., Kosugi T., 1994a, In: Enome S., Hirayama T. (eds.) Proc. of Kofu Symposium, NRO Report No. 360, p. 397
Hudson H.S., Strong K.T., Dennis B.R., et al., 1994b, ApJ 422, L25
Kosugi T., Makishima K., Murakami T., et al., 1991, Sol. Phys. 136, 17
Masuda S., 1994, Ph.D. Thesis, University of Tokyo
Masuda S., Kosugi T., Hara H., Tsuneta S., Ogawara Y., 1994, Nat 371, 495
Masuda S., Kosugi T., Hara H., et al., 1995, PASJ 47, 677
Metcalf T.R., Hudson H.S., Kosugi T., Puetter R.C., Piña R.K., 1996, ApJ 466, 585
Neupert W., 1968, ApJ 153, L59
Ogawara Y., Takano T., Kato T., et al., 1991, Sol. Phys. 136, 1
Peres G., Rosner R., Serio S., Vaiana G.S., 1982, ApJ 252, 791
Sakao T., 1994, Ph.D. Thesis, University of Tokyo
Sato J., 1997, Ph.D. Thesis, Graduate Univ. Advanced Studies
Siarkowski M., Sylwester J., Jakimiec J., Tomczak M., 1996, Acta Astron. 46, 15
Strong K.T., Hudson H.S., Dennis B.R., 1993, In: Uchida Y., Shibata K., Watanabe T., Hudson H. (eds.) X-Ray Solar Physics from *Yohkoh*. Universal Academy Press, Tokyo, p. 65
Tanaka Y., 1983, Sol. Phys. 86, 3
Tandberg-Hanssen E., Emslie A.G., 1988, The Physics of Solar Flares. Cambridge University Press, New York, p. 178
Tomczak M., 1997a, Adv. Space Res 20(12), 2323
Tomczak M., 1997b, A&A 317, 223
Tsuneta S., Acton L., Bruner M., et al., 1991, Sol. Phys. 136, 37